Applied Catalysis B: Environmental 217 (2017) 603–614

Contents lists available at ScienceDirect

Applied Catalysis B: Environmental

journal homepage: www.elsevier.com/locate/apcatb

Research paper

Adsorption and photocatalytic degradation of sulfamethoxazole by a novel composite hydrogel with visible light irradiation

Jianhua Yang[a,b], Zhengkui Li[a,b,*], Hongjie Zhu[a,b]

[a] State Key Laboratory of Pollutant Control and Resource Reuse, Nanjing 210023, China
[b] School of the Environment, Nanjing University, Nanjing 210023, China

ARTICLE INFO

Article history:
Received 2 April 2017
Received in revised form 6 June 2017
Accepted 10 June 2017
Available online 12 June 2017

Keywords:
Composite hydrogel
Sulfamethoxazole
Adsorption
Photocatalytic degradation
Visible light

ABSTRACT

A novel hydrogel catalyst (p(HEA/NMMA)-CuS) with the function of adsorption and degradation of organic pollutants in water was successfully synthesized using irradiation polymerization and in situ precipitation methods The composite hydrogel catalyst was characterized by SEM-EDS, TEM, swelling kinetics, zeta potential, TGA, XPS, FTIR and XRD. Besides, the effects and mechanisms of adsorption and degradation of sulfamethoxazole(SMX) as the representative pollutant by p(HEA/NMMA)-CuS hydrogel were observed. The results presented that adsorption process of SMX on complex hydrogel fit well to Langmuir monolayer adsorption, and followed a pseudo-second-order rate equation. The decomposition of SMX by p(HEA/NMMA)-CuS hydrogel in aqueous solution under 500 w visible light achieved balance in 24 h, the removal ratio reached 95.91%, and the SMX was mineralized with 43.56%. Hydroxyl radicals was detected as the reactive species using EPR in the system, degradation intermediates of SMX were further analyzed by LC-TOF-MSMS, a possible pathway for SMX degradation was presented. The degradation mechanism of SMX was also illustrated by theoretical calculations of frontier electron densities. Furthermore, mineralization, stability and regeneration results indicated that the developed hydrogel catalyst, p(HEA/NMMA)-CuS hydrogel, was promising in practical application.

1. Introduction

Sulfonamide antibiotics(SAs) are well-known aqueous micro pollutants for the difficult degradation, making human and environmental organisms produce resistance to drugs, prompting the continuous emerging of super bacteria [1,2]. Sulfamethoxazole (SMX) as one of the most widely detected SAs in the water resources, has been used as a model SAs in many studies due to its universality, persistence, and toxicity [3]. SMX exists as a cation (SMX^+), neutral molecule (SMX^0) and as an anion (SMX^-) in water, owing to the protonation of the aromatic amine (-NH_3^+-, $pK_a \approx 1.7$) and the dissociation of sulfonamide group (-SO_2NH-, $pK_a \approx 5.7$) [4]. Because of the spatial structure of SMX molecule has a bond angle of 60°, it is vital to know the message of the structure-affinity relationship for adsorption, guide how to design adsorbents and their applications. Therefore, advanced treatment and remediation of wastewater containing sulfonamide antibiotics are urgently needed.

To date, many treatments have been studied in order to remove the antibiotic like SMX in the environmental water, mainly contains physical [5], chemical [6] and biological methods [7]. Adsorption is considered as the convenient operation and green treatment method. Sun et al. [8] studied the sorption of SMX on biochar micropores and found it was mainly via van der Waals and π–π interactions. A high silica zeolite Y was developed by Braschi et al. [9] to the adsorption of SMX through the heterocycle NH of sulfamethoxazole in amide. As an absorbent, hydrogels have excellent properties in the adsorptive of a wide range of aqueous pollutants like heavy metals [10], toxic organics and nutrients [11]. To achieve desired adsorption capacity and selectivity, it is critical to choose more specific interaction sites to remove SMX. In addition, the surface structure of the hydrogel influences its functionality and selectivity, thus the selection of synthetic monomers is also important. There are limited investigations reporting the polymerization hydrogel of *N*-methyl maleic acid(NMMA) and 2-hydroxyethyl acrylate(HEA) with effective functional groups.

Nevertheless, adsorption methods can't reach a completely "eliminate" or "destroyed" [3]. The photocatalysis in chemical measures, because of its simple operation, high efficiency and other advantages of gradually becomes a research focus [12]. So far various photocatalysis were studied, including composite catalysts

* Corresponding author.
E-mail addresses: zhkuili@nju.edu.cn, doctli@163.com (Z. Li).

http://dx.doi.org/10.1016/j.apcatb.2017.06.029
0926-3373/

with carbon nanotubes [13], dyed sensitizers [14], noble metals or metal ions incorporation [15], transition metals [16] and non-metals doping [17]. Among these catalysts, metal semiconductor (TiO_2, ZnO, Fe_2O_3, CdS, CuS, GaP and ZnS et al) catalysts have shown a great potential as an efficient, sustainable treatment technology in the wastewater industry. TiO_2 has been proved to be one of the best photocatalysts [18], but TiO_2 has a large band gap and can't effectively use solar energy [19]. More and more researches on catalysts of visible light responsive had made great efforts, to utilizing solar energy for visible-light degradation of contaminants [20,21]. Some studies have indicated that copper sulfide(CuS) nanoparticles are more responsive to visible light than TiO_2 on the oxidation of organic micro pollutants, and better mineralization rate could be obtained [22,23]. Additionally, considering the methods of preparation and effects of catalyst, copper sulfide nanocrystal material has become one of the hot research topics at domestic and abroad [24]. However, the main technical bottlenecks that hinder its engineering application remained on the recovery and reuse of the catalyst particles [25].

To solve this problem, many materials were studied for catalysis immobilized owing to their structural stability and possible adsorption capacity, including activated carbon [26], mesoporous clays [27], fibers [28], agar [29], nano-silica [30] and polymeric sorbents [31], etc. Herein, the hydrogel as one of high molecular polymer, attracted more and more attentions to the development and application of novel hydrogels in water treatment [11,32]. Additionally, the metal-organic frameworks (MOFs) like photocatalysis based on polymers is being actively investigated [33], as the potential technology in visible light utilizing processes, they could provide an platform for catalytic centers to achieve solar energy conversion [34]. However, the synthesis of three-dimensional (3D) hydrogel structures with photocatalyst copper sulfide nanoparticles for the adsorption and photodegradation organics have been rarely reported. It may be available to synthesis the composite hydrogels of adsorption and photocatalytic properties, to provide a new way for the removal of SMX in wastewater.

Therefore, a novel three-dimensional hydrogel(p(HEA/NMMA)-CuS) with adsorption property and high visible-light catalytic activity was synthesized by ^{60}Co-γ radiation-induced copolymerization and in situ precipitation of copper sulfide. To be a clean and environmental material for the removal of SMX in the water. Moreover, the p(HEA/NMMA)-CuS hydrogel was characterized by scanning electron microscope- Energy Disperse Spectroscopy (SEM-EDS), transmission electron microscopy (TEM), swelling kinetics, zeta potential, X-ray diffraction (XRD), Fourier transform infrared spectra (FTIR), thermo-gravimetric analysis (TGA) and X-ray photoelectron spectroscopy (XPS). Additionally, the study focused specifically on, (i) the adsorption capacity and mechanism of SMX on the p(HEA/NMMA)-CuS hydrogel in water; (ii) the identification of degradation products and possible transformation pathways of SMX in the p(HEA/NMMA)-CuS hydrogel system, (iii) the theoretical and experimental investigation of SMX degradation mechanism under visible light in aqueous solution.

2. Experiment and methods

2.1. Chemicals

SMX ($C_{10}H_{11}N_3O_3S$, CAS NO. 723-46-6, purity 98%) and 2-hydroxyethyl acrylate(HEA) were purchased from Aladdin, USA. *N*-Methyl maleic acid(NMMA) was obtained from Tokyo Chemical Industry (Shanghai, China). All the other reagents used such as $Cu(NO_3)_2{\cdot}3H_2O$ and Na_2S, were all of analytical grade and acquired from Sinopharm Chemical Reagent (Shanghai, China). Methanol and formic acid were of chromatography grade and obtained from Merck (Darmstadt, Germany). The spin-trapping agent 5,5-dimethyl-pyrroline-N-oxide(DMPO) was supplied from Aladdin (Shanghai, China). Ultrapurewater (>18.2 MU cm) was prepared with a Milli-Q Plus system (Millipore, Bedford, USA), and applied all over the paper.

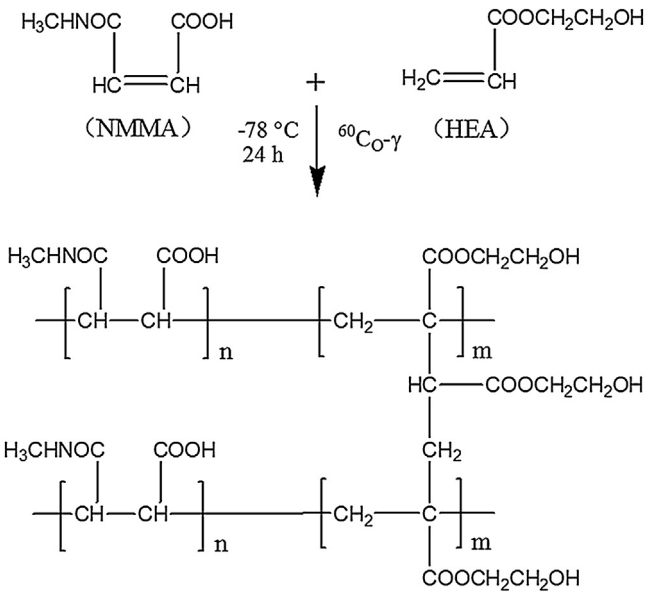

Fig. 1. Scheme for synthesis of p(HEA/NMMA) hydrogel.

2.2. Preparation of hydrogels

2.2.1. Preparation of p(HEA/NMMA) hydrogel

The p(HEA/NMMA) hydrogel was synthetized by the irradiation polymerization method. Fig. 1 presents a possible radiation reaction path of p(HEA/NMMA) hydrogel, in this process, primarily, the mixture of 2 −hydroxyethyl acrylate(HEA) and *N*-methyl maleic acid(NMMA) monomers was prepared with deionized water (v./v. = 3:7), and the molar ratio of monomers was fixed value of 9:1. After that the solution was put in shaker for mixed fully, a nitrogen atmosphere was kept in the process. ^{60}Co-γ radiation-induced copolymerization was employed for 24 h to reach a total dose of 20 kGy, the reaction was operated at −78 °C in dry ice-alcohol system. Finally, the obtained solid hydrogel was washed with deionized water until clean and cut into 5 × 5 × 5 mm dimension of small cubes, then were dried and ready to used.

2.2.2. Preparation of p(HEA/NMMA)-CuS hydrogel

The p(HEA/NMMA)-CuS hydrogel was prepared via loading copper sulfide catalyst on p(HEA/NMMA) hydrogel with in-situ precipitation method, and this in-situ precipitation method was conducted according to Sahiner [35]. Briefly, the dried p(HEA/NMMA) hydrogel cubes was mixed with 40 mM $Cu(NO_3)_2$ solution for 24 h to make sure the Cu(II) ions adsorbed onto p(HEA/NMMA) hydrogel, afterwards, p(HEA/NMMA)-Cu was transferred into 40 mM Na_2S solution for 12 h then washed and dried. The above procedures were carried out at the shaking bath speed of 150 r/min, and temperature of 25 ± 0.5 °C.

2.3. Characterization

SEM (Quanta 250 FEG, FEI, USA) and EDS (Aztec X-MAX^N 80, Oxford, UK) were used to observe the surface feature of p(HEA/NMMA) and p(HEA/NMMA)-CuS hydrogels. FTIR was performed on Bruker Vertex 70 v (Karlsruhe, Germany) in the range of 400–4000 cm^{-1}. TGA was carried out on Pyris 1 DSC (PerkinElmer,

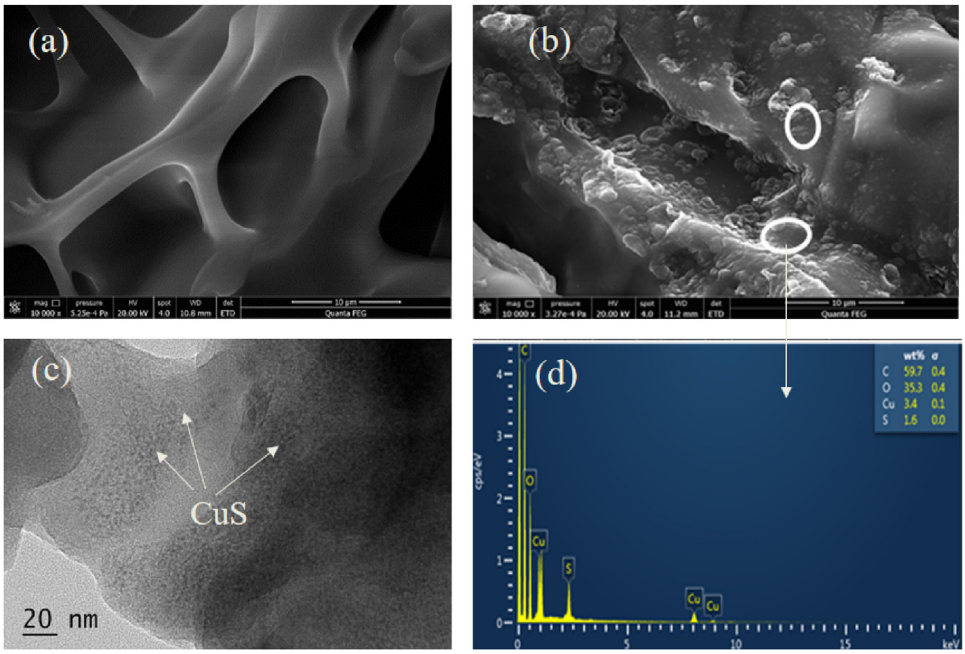

Fig. 2. SEM image of p(HEA/NMMA) hydrogel(a); SEM image (b), EDS (d) and TEM image (c) of p(HEA/NMMA)-CuS hydrogel.

USA), and the temperature was range from 20 to 800 °C at a heating rate of 20 °C min^{-1}. XPS was operated on a PHI-5000 spectrometer (Ulvac-Phi, Japan) in a certain range of 0–4000 eV. X-ray diffraction analysis (D8 ADVANCE, AXS, Germany) at diffraction angle 2θ from 5° to 60° was tested to studied the crystallographic structure.

Swelling kinetics of p(HEA/NMMA) and p(HEA/NMMA)-CuS hydrogels in aqueous phase were observed by the conventional gravimetric analysis method as for our previous study [36], a certain weight of dried hydrogels soaked in water at 25 °C, then swollen hydrogels were weighed by an electronic balance at predetermined intervals. Zeta potential of p(HEA/NMMA) and p(HEA/NMMA)-CuS composite hydrogels were conducted by Zeta PALS/90Plus (Brookhaven, USA), the experiment and measurement methods were on the basis of Wang et al. [37]. The UV–vis diffuse reflectance spectroscopy (DRS) of CuS particle and p(HEA/NMMA)-CuS composite hydrogel were determined by UV-3600 spectrophotometer (Shimadzu, Kyoto, Japan) with a wavelength range of 300–800 nm.

2.4. Adsorption and photocatalytic experiment

Batch adsorption experiments were carried out in order to study the adsorption effect and properties of SMX onto the p(HEA/NMMA) and p(HEA/NMMA)-CuS hydrogels without visible light. Adsorption studies were performed using 50 mg L^{-1} SMX solution of 50 mL in 100 mL conical flask, each of the dried p(HEA/NMMA) and p(HEA/NMMA)-CuS hydrogels of 0.1 g were weighed, and added to the solution for the adsorption process. All the vials were kept without light, then continuously shaken in shaker (150 rpm) at 25 ± 0.5 °C for 24 h.

The experiments of SMX photocatalytic degradation were conducted by using an GHX-V photochemical reactor (Zhengqiao Technology Co., Ltd. Shanghai, China) with a water cooling system. A 500 W Xenon lamp was used as the light source to simulate visible light (390 < λ < 780 nm) in the photocatalysis process, and a 400 nm glass cut-off filter was used to exclude ultraviolet light, the distance between the light source and reaction vessel was adjusted to about 10 cm. A go round apparatus was employed to guarantee uniform light exposure for all solutions. For each experiment, 0.1 g of the dried p(HEA/NMMA)-CuS hydrogel and 50 mL of 50 mg L^{-1} SMX reactant solution were placed in a quartz tube, inserted into the reactor and stirred for 24 h. In the course of irradiation, 1 mL of the solution was taken out at a given time interval, then used for the subsequent determination and analysis of SMX concentration. The equilibrium pH was also measured, and all the reaction process was maintained at room temperature. There was no significant loss of solutes to degradation or adsorption onto vial walls.

2.5. Analytical methods

Agilent 1200 high performance liquid chromatography (Agilent Technologies, Palo Alto, CA, USA) equipped with a UV detector was served to detect the concentrations of SMX at 270 nm. And using a Zorbax 300SB-C18 column (4.6 × 150 mm, 5 μm) for the separation of organics at 25 °C. The mobile phase was consisted of methanol (45%) and 0.1% formic acid in water (55%), the flow rate was 1 mL min^{-1}, and the injection volume was 10 μL.

HPLC/MS method was used for the identification of the degradation products of SMX, it was composed of an Agilent 1260 HPLC and a TOF mass spectrometer (Triple TOF 5600, AB SCIEX, USA). Electrospray ionization (ESI) source in positive ion mode was used as the MS detection, the scanning range of m/z was 70–500. The value of DP and CE were set as 80 and 10, ionspray voltage floating and source temperature were selected as 5500 V and 550 °C. Thermo Scientific Hypersil ODS (C18) Column – Length 100 mm, 2.1 mm ID, 3 μm particle size was used in TOF-5600-MS. All gases used were nitrogen.

EPR (Electron paramagnetic resonance spectrometer) experiments were operated on a Bruker EMX-10/12 spectrometer (Bruker, Germany), and 0.1 M DMPO solution was conducted as a spin-trapping agent for radical measurement [38]. The mixture of the EPR spin trapping experiment contained 1.0 g/L p(HEA/NMMA)-CuS hydrogel and 0.1 M DMPO. After fully mixing, the samples were detected by EPR. DMPO or p(HEA/NMMA)-CuS hydrogel alone were also obtained with the EPR spectra. The spin trapping signals were recorded each 1 min.

The photocurrent characterization of p(HEA/NMMA)-CuS hydrogel was tested on a CHI760E electrochemical workstation (Shanghai, China) with a standard three-electrode system [39]. The

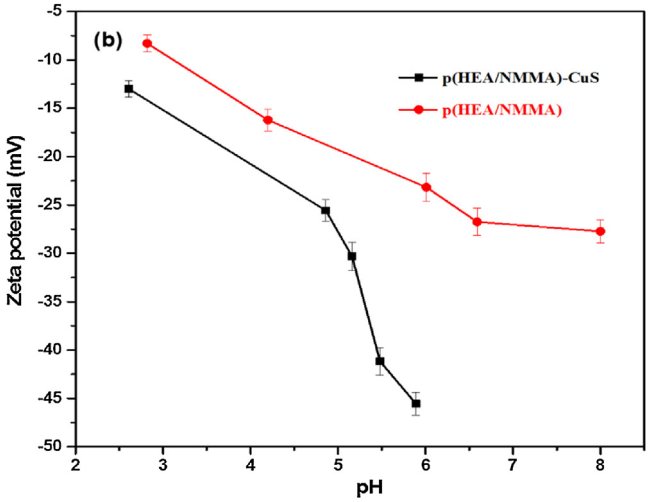

Fig. 3. Zeta potentials of p(HEA/NMMA)-CuS hydrogel, as compared with those of p(HEA/NMMA) hydrogel.

ITO electrode (1 cm × 2 cm squares) was employed to load the samples and as the working electrode. Ag/AgCl electrode and Pt plate were served as reference electrodes and the counter, respectively. 0.1 M Na_2SO_4 aqueous solution was used as electrolyte and a 500 W xenon lamp was selected as the light source.

A Shimadzu TOC-5000 total organic carbon analyzer (Shimadzu, Kyoto, Japan) was used to determine the Total organic carbon (TOC) values of the solutions. The UV-2450 (Shimadzu, Kyoto, Japan) was used to detect the absorption of substances in aqueous solution at different wavelengths. In this article, to predict the possible degradation pathways of SMX in aqueous phase, the geometries of SMX were optimized by the DFT-B3LYP/6-311G (d, p) method, the theoretical calculations of quantum properties were performed using Gaussian 09 program [40]. The frontier electron density ($FED^2$of SMX) was calculated with the Multiwfn3.3.9 software.

3. Results and discussion

3.1. Characterization of catalysts

3.1.1. SEM, EDS and TEM

The SEM images of p(HEA/NMMA) hydrogel carrier (a) and p(HEA/NMMA)-CuS hydrogel (b), as well as EDS (d) and TEM(c) images of p(HEA/NMMA)-CuS hydrogel were shown in Fig. 2. As presented in Fig. 2(a), the p(HEA/NMMA) hydrogel carrier have a smooth surface and structure of 3D macro-porous network, the irregularly shaped macropores ranged from 10 μm–50 μm in the size, densely distributed in the copolymer hydrogel. When copper sulfide particles were lorded on the p(HEA/NMMA) hydrogel (Fig. 2(b and c)), countless nanoparticles were observed on the surface and network of the hydrogel, the roughness of p(HEA/NMMA)-CuS hydrogel improved obviously. It could be confirmed that the presence of copper and sulfur elements on the hydrogel surface as depicted in Fig. 2(d) from EDS spectrum, in different part of the hydrogel, the loading density was almost same. The particle size was further evaluated by TEM (Fig. 2(c)), the results indicated that CuS particles were loaded as nanometer level on p(HEA/NMMA) hydrogel, and CuS nanoparticles slightly gathered in the hydrogel carrier.

3.1.2. Zeta potentials

The zeta potentials of p(HEA/NMMA)-CuS composite hydrogel and p(HEA/NMMA) hydrogel under different solution pH values were depicted in Fig. 3, they all exhibited negative zeta potentials over a pH value range from 2 to 8. The zeta potentials of p(HEA/NMMA)-CuS hydrogel were lower than p(HEA/NMMA) hydrogel at different pH values, suggesting that p(HEA/NMMA)-CuS hydrogel has higher charged densities. To our knowledge, the pK_a of SMX is about 1.7 for the protonation of the aromatic amine, and about 5.7 for the dissociation of sulfonamide group [41]. At pH ≤ 5.7, the majority of SMX are neutral, the adsorption between the hydrogel and SMX may be due to H bonding interactions. At pH > 5.7, the SMX mainly as anion, adsorption maybe occurred between pollution and hydrogels via the interaction of electrostatically, or say electrostatic action plays a mainly part [4].

3.1.3. UV–vis analysis and photocurrent

To study their absorption properties of visible light and band gap evaluation, the CuS nanoparticles and p(HEA/NMMA)-CuS hydrogel were analyzed by diffuse reflectance spectroscopy. As can be seen in Fig. 4(a), the p(HEA/NMMA)-CuS hydrogel possessed a better absorption compared with that of pure CuS nanoparticles at the visible wavelength range of 520–800 nm, revealing the composite hydrogel catalyst should have an excellent visible light catalytic property. Moreover, the band gap energy of CuS nanoparticles and p(HEA/NMMA)-CuS hydrogel were evaluated from the diffuse reflectance spectroscopy by the following equation [39]:

$$\alpha h\nu = A(h\nu\text{-}E_g)^n \quad (1)$$

Where α, A and hν represent the absorption coefficient, constant and photon energy, respectively. E_g is the optical band gap energy, the value of n lies on whether the electronic transition is direct (n = 1/2) or indirect (n = 2). The value of n equals 1/2 for CuS nanoparticles [42,43]. Through extrapolating the linear portion of the $(\alpha h\nu)^2$ versus hν curves to the energy axis at α = 0, the band-gap energies were estimated as shown in Fig. 4(b). The E_g of CuS nanoparticles and p(HEA/NMMA)-CuS hydrogel was about 2.37 eV and 1.88 eV, respectively. The reduction of E_g value of p(HEA/NMMA)-CuS hydrogel illustrating a wider optical absorption scope than pure CuS nanoparticles, implying more electron–hole pairs may be generated with the same visible light irradiation [44].

Photocurrent determination of p(HEA/NMMA)-CuS hydrogel was conducted to investigate the separation performance of photogenerated electron-hole pairs. Usually, the value of photocurrent indirectly represented the capacity of generating and transferring the photo-excited charge carrier, which related to the photocatalytic activity [45]. As shown in Fig. 10(b), with the visible light turn on and off, the photocurrent displayed a relatively stable trend, indicating that the electrons and holes generated by p(HEA/NMMA)-CuS hydrogel could be separated during the degradation of SMX.

3.1.4. Other characterization

The swelling ratio of synthesized polymer hydrogel, is not only related to the gel hydrophilic, the number of hydrophilic groups, the pore size and crosslinking degree of hydrogel, but also the surrounding conditions especially pH value and temperature [46] [47,48]. The swelling kinetics of the p(HEA/NMMA) hydrogel and the p(HEA/NMMA)-CuS hydrogels in ultrapure water and in SMX solution were exhibited in Fig. S1(a) and (b), respectively. The swelling ratio increased after loading CuS nanoparticles, but the extent of increasing was different with the specific conditions. The reason may be that the grid structure of p(HEA/NMMA)-CuS hydrogel was improved as well as the surface roughness and hydrophilic of hydrogel were elevated for the proper amount presence of copper sulfide nanoparticles. This feature made it easier for the liquid diffusion and the SMX molecules interact with functional groups on hydrogel.

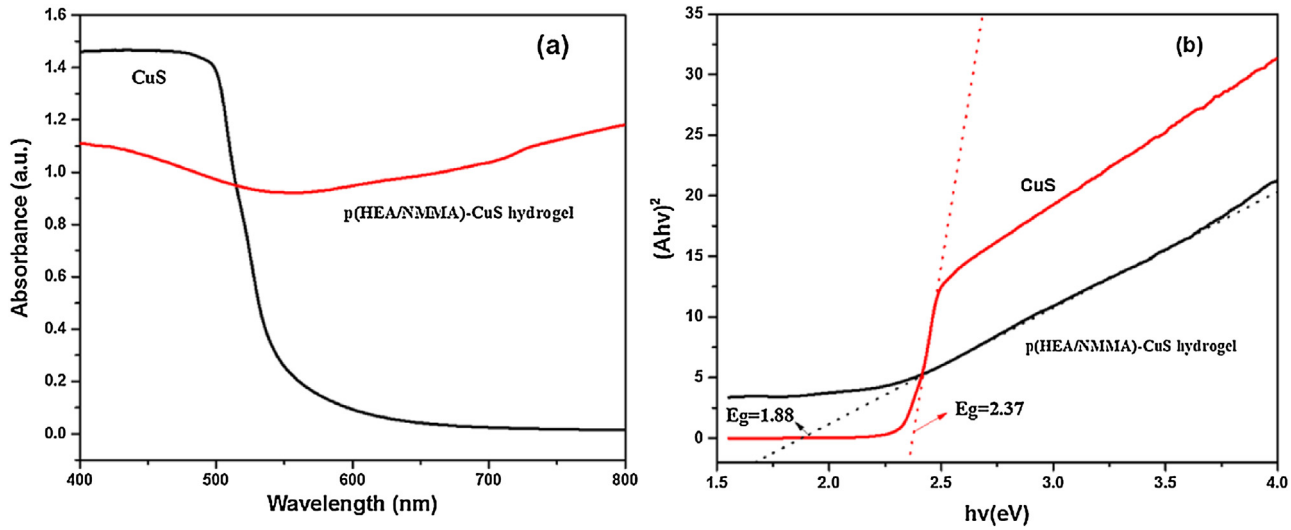

Fig. 4. (a) UV–vis diffuse reflectance spectra of CuS particles and p(HEA/NMMA)-CuS hydrogel, (b) The band gap evaluation for linear dependence of $(Ahv)^2$ versus hv for CuS particle and p(HEA/NMMA)-CuS hydrogel.

As depicted in Fig. S2. The TGA thermograms of HEA, p(HEA/NMMA) and p(HEA/NMMA)-CuS hydrogels (Fig. S1, Supporting information) were carried out. The result showed that HEA had only one sharp weight loss at about 196 °C, and a three-step weight loss were observed for p(HEA/NMMA) and p(HEA/NMMA)-CuS hydrogels. It was reported in a previous study that the first step of weight loss is the physically adsorbed water [32], up to 236 °C, there is around 10–15 wt% weight loss of hydrogels, and it's obvious that the improved hydrophilic of the p(HEA/NMMA)-CuS hydrogels than p(HEA/NMMA) hydrogel. The second step of thermal process was continued from 236 °C to 352 °C, the reaction of dehydration occurred. Then, the third step started from 352 °C to 800 °C, the weight loss was largely due to splitting of the polymer main chain. The last remaining around 10% weight of p(HEA/NMMA)-CuS hydrogel is the inorganic particles, indicating that the hydrogel contains about 10 wt% CuS nanoparticles.

The FTIR spectra of p (HEA), p(HEA/NMMA) and p(HEA/NMMA)-CuS hydrogels were determined in order to identify the existence of functional groups (Fig. S3). The XPS spectra of p(HEA/NMMA)-CuS hydrogel (Figs. 6 and 7) were showed to further confirm the structure of the hydrogel, the XRD (Fig. S4) pattern were also performed. All the above characterization results indicating that CuS nanoparticles had been successfully and firmly loaded on hydrogel carriers.

3.2. Adsorption properties

3.2.1. Adsorption kinetic experiment

As presented in Fig. 5(a), adsorption kinetics experiments of SMX on p(HEA/NMMA) and p(HEA/NMMA)-CuS hydrogel within 6 h were conducted at room temperature. During the first 30 min, the adsorption amounts increased rapidly with time, then the rate of adsorption gone to slowly until equilibrium approximately in 4 h. Moreover, the adsorption capacity of SMX on p(HEA/NMMA)-CuS hydrogel increased obviously compared to p(HEA/NMMA) hydrogel, it was improved about 66.2% from 2.32 mg/g to 3.86 mg/g. Fig. 5(b) shows the adsorption kinetic model of SMX on the p(HEA/NMMA)-CuS hydrogel, because of the high correlation coefficients ($R^2 > 0.999$), the approximation between the calculated equilibrium adsorption capacity ($Q_{e,c}$) and the testing adsorption capacity ($Q_{e,e}$), illustrated that SMX adsorption onto p(HEA/NMMA)-CuS hydrogel could be approximately favorable by the pseudo-second-order model, but pseudo-first-model showed fitting not well. Therefore, the adsorption of SMX

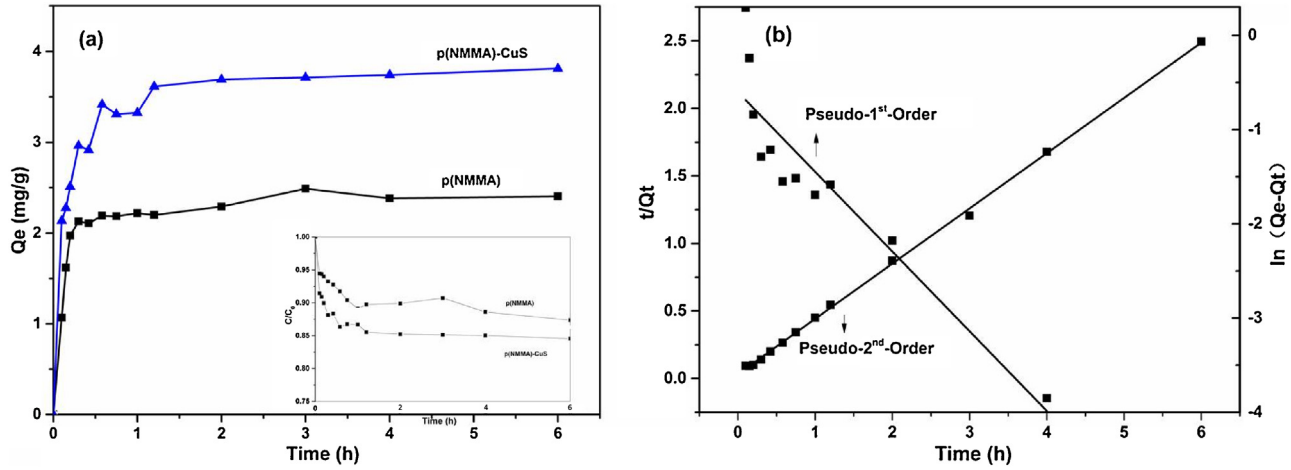

Fig. 5. (a) Adsorption kinetic of SMX on p(HEA/NMMA) and p(HEA/NMMA)-CuS hydrogel. Inset: The plots for SMX removal rate of p(HEA/NMMA) and p(HEA/NMMA)-CuS hydrogel. Conditions: $[SMX]_0 = 0.2$ mM, $pH_0 = 3.0$, 25 °C. (b) Adsorption kinetic model of SMX on the p(HEA/NMMA)-CuS hydrogel.

on p(HEA/NMMA)-CuS hydrogel may be a chemical process, functionalities play the major role in adsorption, as compared to the structural characteristics of hydrogels [37].

3.2.2. Adsorption isotherm experiment

The adsorption isotherm results of SMX on p(HEA/NMMA)-CuS hydrogel was depicted in Fig. S5(a). The results indicated that with the increasing of initial SMX concentration, the equilibrium adsorption capacity of SMX on the p(HEA/NMMA)-CuS hydrogel was also enhanced significantly, until reached the maximum adsorbed amount of 31 mg/g at 2 mM. Fig. S5(b) showed that the adsorption of SMX on p(HEA/NMMA)-CuS hydrogel could be described by Langmuir model well, indicating it was monolayer adsorption on homogeneous surface at constant temperature [11], and Freundlich model did not show a good fit. Similarly, Lan et al. found that SMX molecules mainly showed positive and neutral in aqueous solution at pH 2.0 and 4.0, and the adsorption of SMX onto Carboxylic-Functionalized Carbon Nanofibers-Encapsulated Ni Magnetic Nanoparticles more close to Langmuir model [4]. Due to the presence of specific functional groups in monomers (having charge opposite to that of pollutant), such as hydroxyl of HEA, amide and carboxyl of NMMA, functional groups or electrostatic interactions may be the main mechanism in the removal of SMX using hydrogels.

3.2.3. Adsorption mechanism and possible process

To further confirm the adsorption mechanism, the high-resolution XPS spectrums of the p(HEA/NMMA) hydrogel and p(HEA/NMMA)-CuS hydrogel before and after the adsorption of SMX were explored. As the results presented (Fig. 6) of the p(HEA/NMMA) hydrogel, there was no obvious change with the peak of O1s before and after the adsorption of SMX. A new peak of S 2p emerging at 167.5, illustrating the SMX has been absorbed on p(HEA/NMMA) hydrogel. Furthermore, the peak of N1s at 391.9 disappeared after the adsorption of SMX on p(HEA/NMMA) hydrogel, indicating the energy site of N1s at 391.9 was taken up or replace by SMX molecules, which may be attributing to the function of amide group on the NMMA monomer.

As for the adsorption of SMX on the p(HEA/NMMA)-CuS hydrogel, Fig. 7 illustrates that no remarkable variety with the peak of O1s and N 1s before and after the adsorption of SMX. Similarly, a new peak of S appearing at 166.5 after the adsorption of SMX, confirming the SMX absorbed on p(HEA/NMMA)-CuS hydrogel. However, the peak of Cu at 930 disappeared after the adsorption of SMX on p(HEA/NMMA)-CuS hydrogel, indicating the energy site of Cu at 930 was taken up or replace by SMX molecules. It was explained that not only the amide groups on the hydrogel carrier can adsorb SMX, the CuS nanoparticles also can adsorb SMX through some chemical bond.

Based on the above results, the adsorption process could be inferred briefly. At the initial stage, the mass transmit of SMX was one important step. With the constant swelling of hydrogels, SMX molecules diffused into the channels of p(HEA/NMMA) and p(HEA/NMMA)-CuS hydrogels, then stayed on the surface or the pore of the hydrogels as a reversible adsorption process. Afterwards, during the slow fraction process, the kinetic velocity conformed to the pseudo-second-order model, SMX molecules were trapped by special function groups or through chemical bond on the hydrogels. Finally, the adsorption of SMX reached saturation and equilibrium.

With above analysis, reasons for the adsorption capacity of the p(HEA/NMMA)-CuS hydrogel is higher than the p(HEA/NMMA) hydrogel may be find. On the one hand, it is probably for the higher swelling ratio of p(HEA/NMMA)-CuS hydrogel, made it easier for more SMX molecular interact with the amide functional groups on hydrogel. On the other hand, besides the adsorption of SMX by the amide groups on hydrogel carrier, there are still some CuS nanoparticles on the composite hydrogel adsorb SMX through some chemical bond. Thus, the adsorption of SMX onto p(HEA/NMMA)-CuS hydrogel might be attributed to their combined effect.

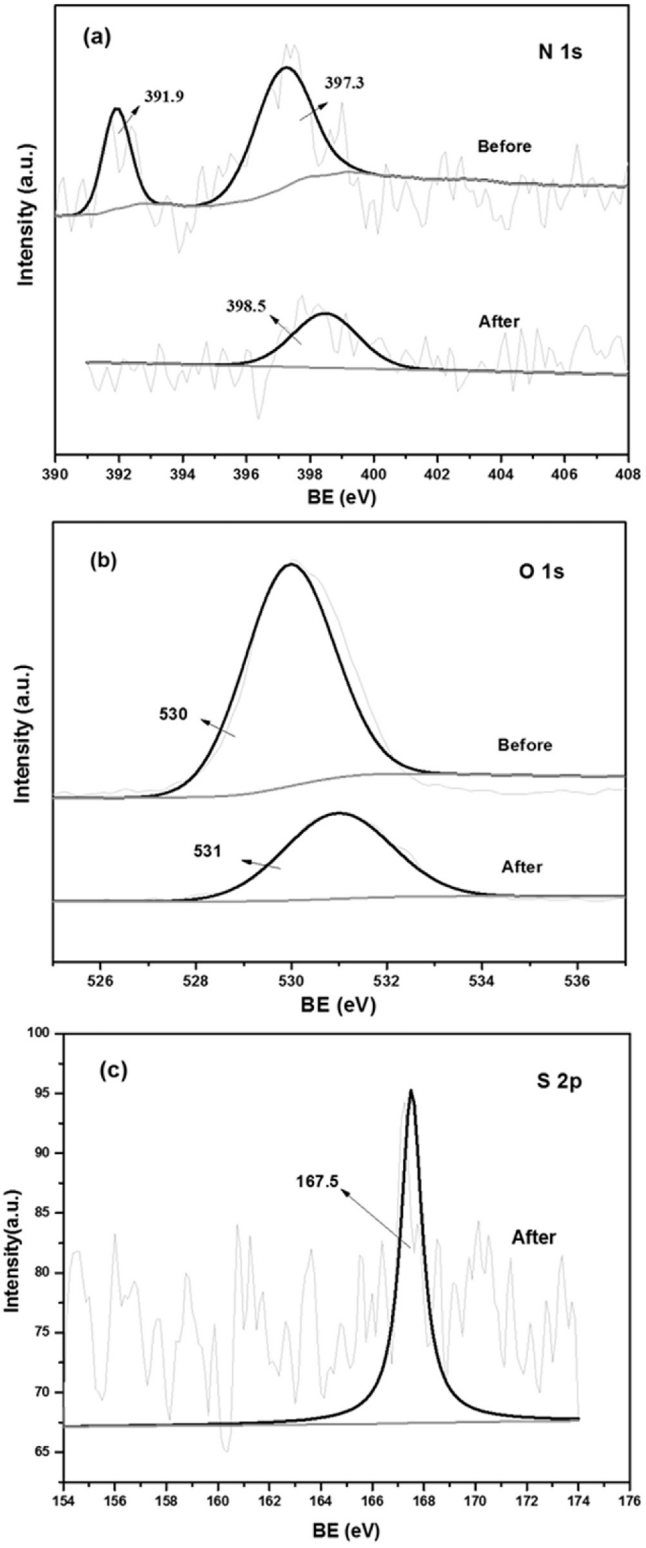

Fig. 6. High-resolution XPS spectra((a) N 1s, (b) O 1s, (C) S 2p) of p(HEA/NMMA) hydrogel before and after the adsorption of SMX. Adsorption conditions: $[SMX]_0 = 0.2$ mM, $pH_0 = 3.0 \pm 0.2$, 25 ± 0.2 °C.

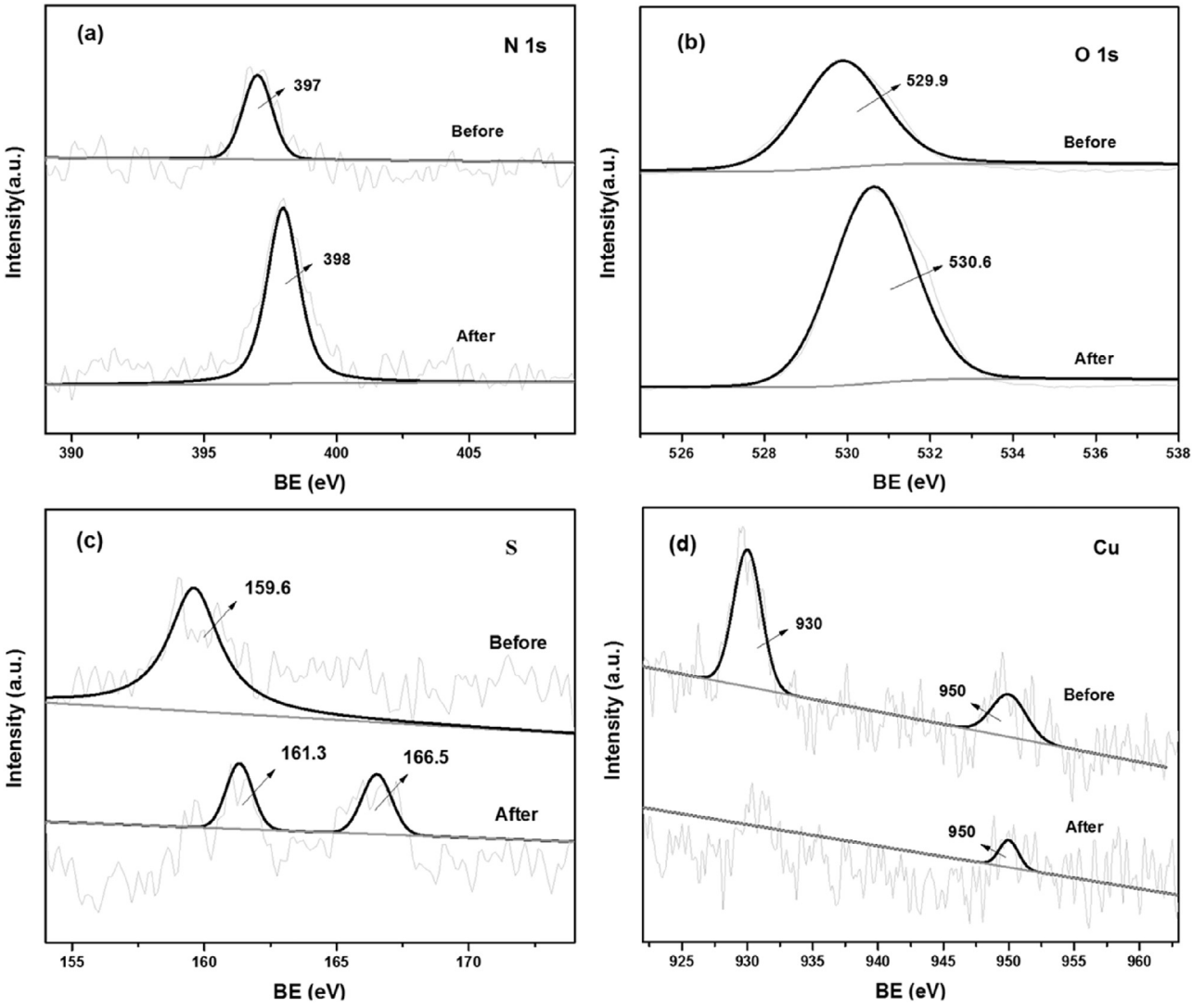

Fig. 7. High-resolution XPS spectra((a)N 1s, (b) O 1s, (c) S, (d) Cu) of p(HEA/NMMA)-CuS hydrogel before and after the adsorption of SMX. Adsorption conditions: $[SMX]_0 = 0.2$ mM, $pH_0 = 3.0 \pm 0.2$, 25 ± 0.2 °C.

In adsorption process, the pH value of SMX solution is also a critical parameter, as a result of the chemical form of SMX at diverse pH level. Fig. S6 presents the influence of pH value on the SMX adsorption quantity onto p(HEA/NMMA)-CuS hydrogel, there was a lower adsorption capacity of SMX with the raise of initial pH, it is approximate 4 mg/g at pH 5–7. Similarly, the adsorption capacity of SMX was 3.17–4.35 mg/g using Fe_3O_4-GO as magnetic solid-phase extraction adsorbent [5]. Considering the adsorption effect of SMX and the application range of pH, the pH value of 3 was chosen as reference to study the effect of SMX degradation. The following studies of the SMX degradation by p(HEA/NMMA)-CuS hydrogel in aqueous phase were all under this condition.

3.3. Degradation efficiency of SMX

To estimate the catalytic oxidation ability of SMX on p(HEA/NMMA)-CuS hydrogel catalysts, degradation kinetics of SMX under 500W visible light were carried out, as Fig. 8(a) shown, SMX was degraded by 0.1 g p(HEA/NMMA)-CuS hydrogel catalysts and 90.91% was eliminated within 12 h. However, Gong and Chu reported that SMX was removed about 55% with UV irradiation in 5 h at the same concentration [49]. The biodegradation removal efficiencies of SMX would be only 9.9–17.1% in the reactors for 48 h [50]. Therefore, there are obvious high degradation effect of SMX on p(HEA/NMMA)-CuS hydrogel. In the former 2 h, the 40% of SMX in solution was rapidly degraded and then the degradation rate became slowly until equilibrium approximately in 12 h. Compared to the degradation, adsorption process of SMX without visible light (Fig. 8(a)) showed a lower removal effect, about 17.50% was adsorbed within 2 h and then reached adsorption equilibrium.

The K_{obs} of SMX degradation was 0.1864 h^{-1} ($R^2 = 0.99$) as Fig. S7 displayed. Such degradation rate might be mainly determined by two aspects, one was the loading quantity of copper sulfide, the other may be the adsorption amount of hydrogel. The influence of visible light intensity on photodegradation of SMX was also observed as Fig. S8 present, the results suggested that degradation efficiency was significantly affected by visible light intensity. When the irradiation intensity of visible light was 500 W, 300 W and 100 W, the degradation efficiency of SMX was 95.90%, 74.90% and 45.47% in 24 h, respectively. The degradation efficiency decreased with the reduction of visible light intensity. This result was similar to some studies [25,51], below some threshold value of the light intensity, light intensity is still one of the factors that could effect on the extent of photocatalytic degradation of organic maters.

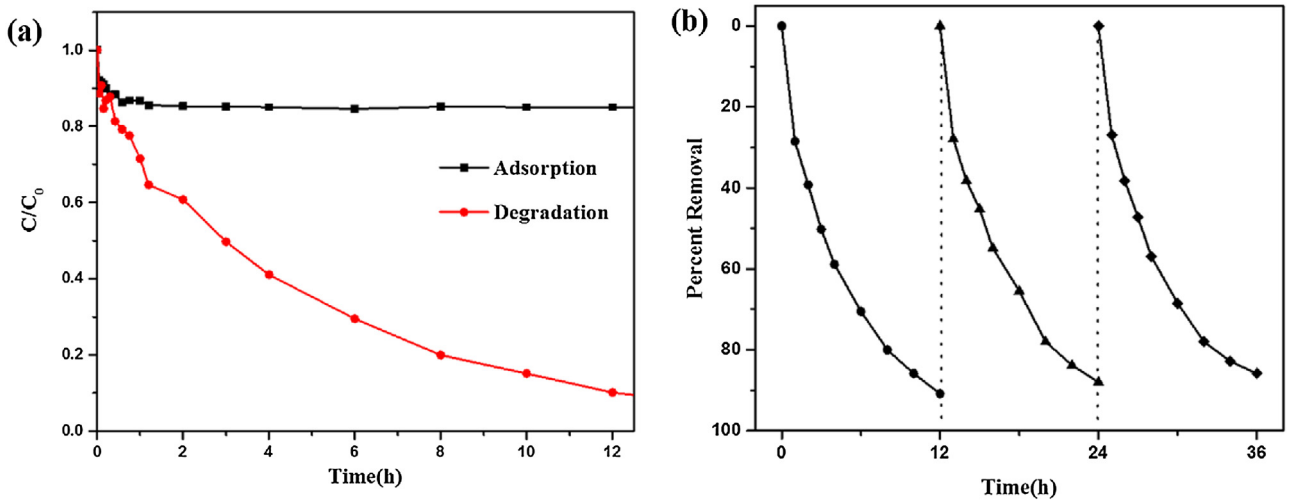

Fig. 8. (a) Adsorption process without visible light and photocatalystic degradation kinetics of SMX under 500W visible light; (b) Cycling runs for the photodegradation of SMX over p(HEA/NMMA)-CuS hydrogel. Condition: 0.1 g hydrogel, 0.2 mM SMX.

3.4. Degradation products and proposed pathways studies

3.4.1. Products analysis

The major degradation products were identified by LC/MS in positive mode. It showed a good agreement (<3 ppm error) between the proposed molecular formulas and the accurate mass measurements, a high degree of certainty was guaranteed in the structural assignments. Eight primary intermediates of SMX degradation in the hydrogel catalysis system, including P1(*m*/*z* 98.9), P2(*m*/*z* 107.9), P3(*m*/*z* 155.9), P4(*m*/*z* 172.9), P5(*m*/*z* 237.9), P6(*m*/*z* 275.9), P7(*m*/*z* 264.9) and P8(*m*/*z* 305) were provided. As shown in Fig. S9, S10, their MS data and proposed structures were provided. P1 was determined as 3-amino-5-methylisoxazole [52], which was due to the cleavage of S-N bond in SMX, accompanying with P1, the other product P3 would also be yielded, they were also detected by Liu et al. as an intermediate in the Fenton-like degradation process of SMX [53]. In addition, P4 was regarded as the addition of hydroxyl group to P3, this agrees with the results from Gong and Chu [49]. P2 was confirmed as the hydroxylated derivative of the product attributed to the break of S-C bond in P3, P5 was generated via deamination reaction of SMX, and P6 was the sodium salt of SMX. P7 was considered as the oxidation of the amine group at the benzene ring on SMX, which inferred from the results of Wang and Helbling [54], the sodium salt of the nitration of amino group on SMX was conformed to P8. The identification of P5, P7 and P8 suggested the amino group (-NH_2) on the aromatic ring of SMX was susceptible to be attacked by reactive radicals.

3.4.2. Theoretical calculation

Besides experimental researches on the degradation mechanisms of SMX by p(HEA/NMMA)-CuS hydrogel in aqueous, theoretically by calculating the frontier electron densities (FEDs) were also studied. Depending on frontier orbital theory, it was most easily attacked by electrophilic or oxidizing reagents at the position of the largest value of Fed^{2}HOMO [40]. Therefore, the distribution of the FED$^2_{HOMO}$ in SMX were computed to forecast the sites for attack of hydroxyl radicals, and the results are shown in Table 1. As the structure of SMX was presented in Fig. 9(b) and the calculated results demonstrated that the larger FED^{2}HOMO values are the position of S7, N10, N17 and C atoms in the benzene ring (C1, C3, C4 and C5). The S7 and C atoms of the benzene ring (C1, C3, C4 and C5) should be the sites where the electrons are extracted by the hydrogel photocatalysis, and bring about the destruction of the amine group and benzene ring on SMX, then these intermediate products will be continuously attacked by hydroxyl radicals. The computed isodensity surfaces of the FMOs (HOMO and LUMO) of SMX were shown in Fig. S11.

Table 1
Frontier electron densities (FED$^2_{HOMO}$) on atoms of SMX.

Atoms	FED$^2_{HOMO}$	Atoms	FED$^2_{HOMO}$	Atoms	FED$^2_{HOMO}$
C^1	**19.59%**	S^7	**1.21%**	C^{13}	1.22%
C^2	2.08%	O^8	0.90%	C^{14}	0.14%
C^3	**11.25%**	O^9	0.82%	C^{15}	0.26%
C^4	**11.11%**	N^{10}	**5.66%**	C^{16}	0.03%
C^5	**12.74%**	O^{11}	0.80%	N^{17}	**28.42%**
C^6	1.76%	N^{12}	**2.22%**		

Larger FED$^2_{HOMO}$ values were shown in bold.

Additionally, the above results of theoretical calculation and analysis of degradation products, indicated that the N—S bond, N—C bond, C—S bond, and the C—C bond (benzene ring) in SMX molecule, were easily broken by the attack of hydroxyl radicals. Therefore, the degradation of SMX by the hydrogel photocatalysis mainly arise from both the cleavage of the N—S bond and the break of the benzene ring; the hydroxyl radicals continued to react with intermediate products, until the SMX were completely mineralized.

3.4.3. Possible pathway

Based on the above results on the oxidation products and chemical structures of the intermediates of SMX, possible degradation pathways of SMX on p(HEA/NMMA)-CuS hydrogel in solution were preliminary proposed. The radicals or holes could attack the sites of S—N bond, benzene ring and amine group on the aromatic ring in SMX, respectively. According to the literature [55] and experimental results obtained, the possible pathways of the visible light degradation for SMX can be proposed here (Fig. 9(a)). Mainly three possible degradation pathways taken place in the process of photocatalytic degradation, the cleavage of S—N bond, oxidation of amino group on the aromatic ring [53], and desamination.

3.5. Potential process mechanism

3.5.1. Radical detection

As well known, the highly reactive oxygen species (ROS) were generated owing to the photo-induced charge separation on the surface of catalysts, then lead to the occurrence of the degraded and mineralization of organics. In order to understand the mainly role in the degradation process, the reaction system was detected

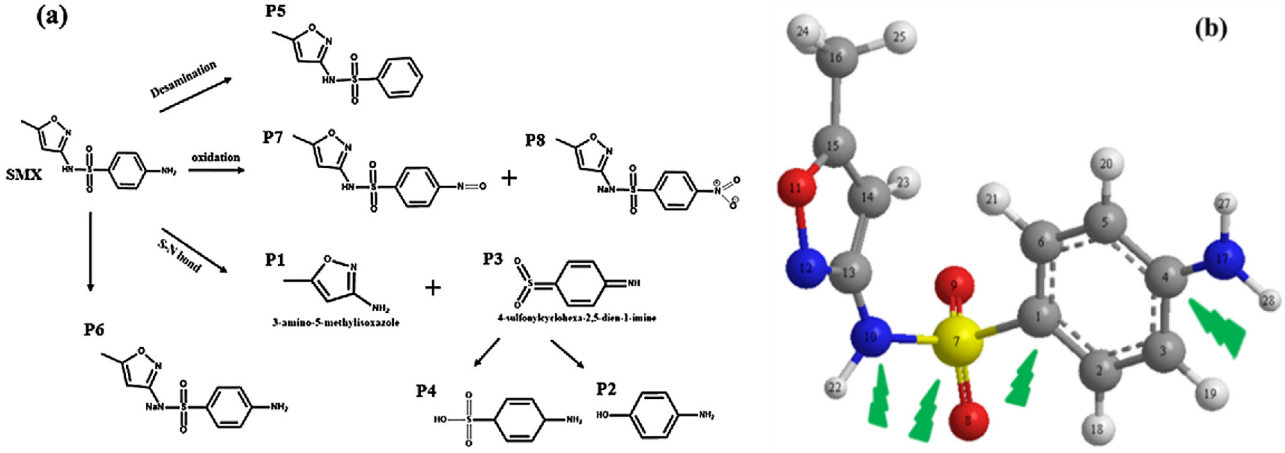

Fig. 9. (a) Proposed degradation pathways for the oxidation of SMX on p(HEA/NMMA)-CuS hydrogel in aqueous solution. Conditions: $[SMX]_0 = 0.2$ mM, $pH_0 = 3.0 \pm 0.2$, 25 ± 0.2 °C. (b) Molecular structure and spatial position of each element of SMX.

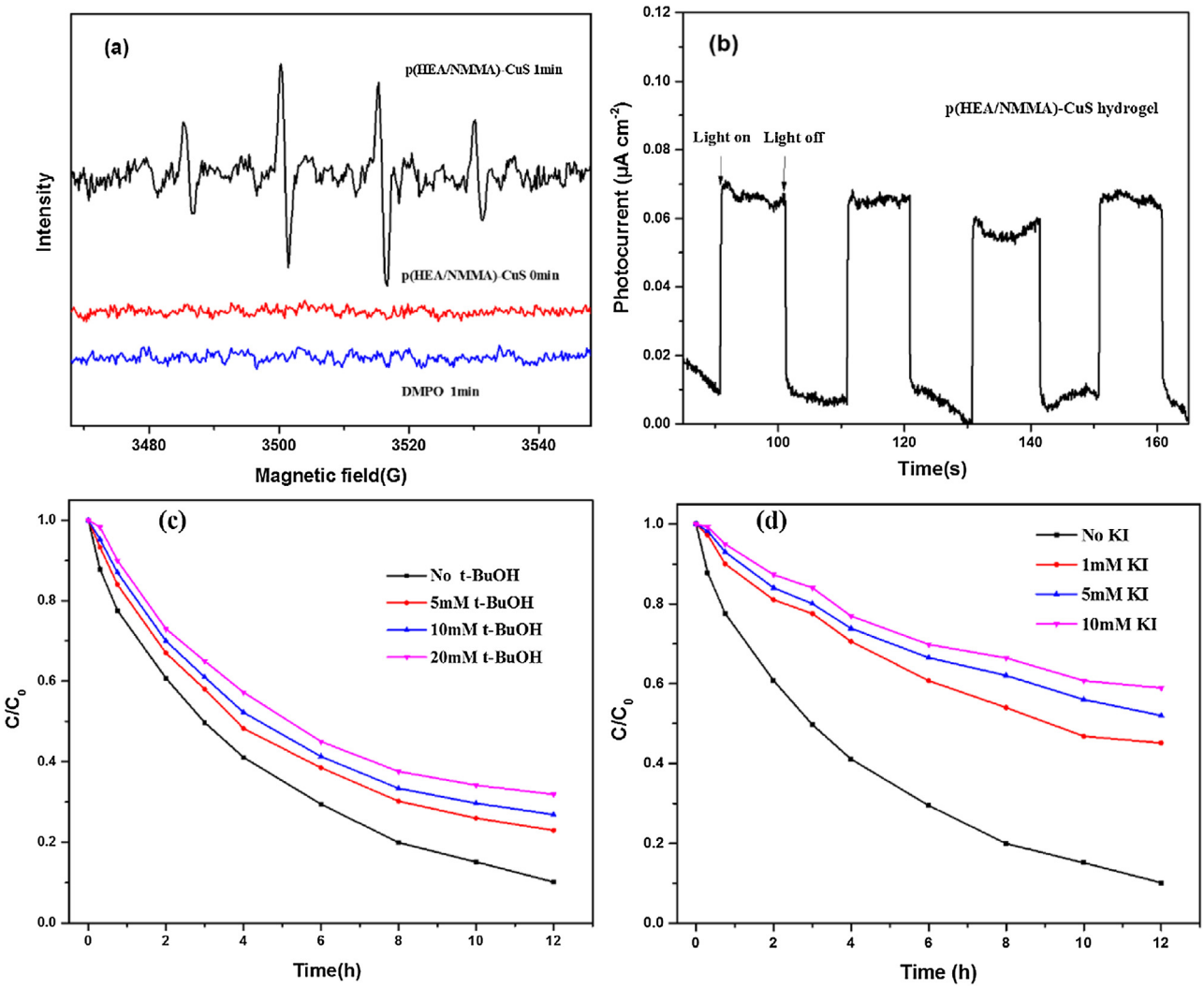

Fig. 10. (a) EPR spectrum of DMPO-OH adducts in solution with p(HEA/NMMA)-CuS at 0 min, 1 min and only DMPO at 1 min under visible light irradiation; (b) Photocurrent of p(HEA/NMMA)-CuS hydrogel under visible light irradiation($\lambda > 450$ nm); Effects of t-BuOH (c)and KI (d) on the photodegradation of SMX by p(HEA/NMMA)-CuS hydrogel under 500W visible light.

by EPR. As presented in Fig. 10(a), four typical characteristic peaks with a strength ratio of 1:2:2:1 were detected in the EPR spectra of p(HEA/NMMA)-CuS hydrogel catalyst system, that was with the presence of 0.1 M DMPO at 1 min under visible light irradiation. While no signal was observed without visible light irradiation, also no obvious signal peak was found in the pure DMPO solution

at 1 min under visible light irradiation. The result clearly illustrated that •OH was the active species for SMX degradation on p(HEA/NMMA)-CuS hydrogel catalyst in aqueous solution [38].

In order to confirm the contribution of h^+ and the predominant reactive species during the degradation process, effects of t-BuOH and KI on the photodegradation of SMX were explored by p(HEA/NMMA)-CuS hydrogel under 500 W visible light. In this experiment, t-butyl alcohol (t-BuOH) and KI were used as the scavenger of •OH and h^+, respectively [45]. As depicted in Fig. 10(c) and (d), with the adding of t-BuOH in reaction solution, the degradation effective of SMX exhibited slightly decreased. It may be that the effect of •OH was limited in the degradation of SMX. Nevertheless, the degradation effective of SMX was significantly inhibited with the presence of KI during the process, suggesting that the h^+ played an important role during the degradation process of SMX. Meanwhile, the more addition of scavengers, the more suppression of degradation.

3.5.2. Underlying mechanism

As far as we know, the optical band-gaps of CuxS were belong to visible light response intensity range, CuS can absorb maximum solar energy among the CuxS [22]. Herein, the band gap of CuS nanoparticles was 2.37 eV through calculation. To obtain the band structure of CuS nanoparticles, which associated with the photocatalytic property. The valence band (VB) and conduction band (CB) potentials of CuS nanoparticles at the point of zero charge were calculated, and following the Eqs. (2) and (3) [39]:

$$E_{CB} = X - E^e - 1/2E_g \quad (2)$$

$$E_{VB} = E_{CB} + E_g \quad (3)$$

Where X, E^e and E_g is the absolute electronegativity of CuS, the energy of free electrons on the hydrogen scale (4.5 eV) and the band-gap energy of CuS, respectively. According the above calculation, the potential value of E_{VB} and E_{CB} of CuS was 1.98 eV and −0.39 eV, respectively.

Additionally, compared to the standard reduction potential of •OH/OH^- (2.38 eV) or •OH/H_2O (2.27 eV), the E_{VB} (1.98 V) of CuS is not positive enough. Hence, the most h^+ generated on CuS may can't oxidize OH^- or H_2O into •OH. With the above results, it was the h^+ played the primary role in the photocatalytic degradation of SMX. One side, the holes oxidized and degraded SMX directly, on the other hand, through the formation of partial •OH by holes to degraded SMX indirectly. Therefore, in the course of the degradation of SMX, the holes played a major role in oxidation and •OH made an auxiliary role.

Thus in this system, visible light directly excited the copper sulfide nanoparticles to start the degradation reactions, while the major role of the CuS particles in general was medium of electron transfer. During this process, the visible photocatalysis generated holes, which were able to oxidize H_2O to •OH and directly degraded the organic contaminants. Due to the strong oxidizing power of the holes, the organics could be completely mineralized through the oxidation reactions.

On the basis of the above results, including the adsorption properties, the analysis of degradation products, the detection of reactive oxygen species and the inference of possible degradation path. It can be briefly concluded as following: First of all, owing to the chemical capture by amide and CuS nanoparticles on the hydrogels, SMX molecules adsorbed on the composite hydrogel and pore surface, contacted with the CuS nanoparticles on the hydrogel. At the same time, under visible light irradiation, electrons and holes generated by the visible light excitation of CuS nanoparticles, then hydroxyl radicals were generated by the oxidation of the OH^- and the H_2O molecules. Finally, the holes and •OH radicals continuously attack the SMX into small molecule, until it is completely degraded into water and CO_2.

3.6. The mineralization and stability

During the SMX oxidation process, the TOC removal was determined to observe the mineralization of SMX (Fig. S12). The results indicated that the mineralization of SMX on the novel composite hydrogel reached to 43.56% when degradation equilibrium, the degradation of SMX was concluded by mineralization to CO_2 and H_2O. As we know, Ghauch et al. studied the degradation of SMX in the Fe0/PS system, and the mineralization rate of SMX was 37% [6]. About 5% removal efficiency of TOC decay with UV illumination in 5 h, while it was 50% removal of TOC with the catalyst (UV/$CoFe_2O_4$/TiO_2) [49]. This was probably a good consequence of the TOC removal of SMX by the p(HEA/NMMA)-CuS hydrogel.

Cycling tests were performed to evaluate the stability of the p(HEA/NMMA)-CuS hydrogel, the used hydrogel was gathered from the reaction solution, then washed by ultrapure water to reuse. As Fig. 8(b) presented, it was found that the photocatalytic activity of the p(HEA/NMMA)-CuS hydrogel presented slight decrease after three continuous cycles of visible light photocatalytic experiments (from 90.91% to 85.60%), indicating that the composite hydrogel had the advantages of separation-free and easy to recycle. In addition, to explore the structural stability, modulus of elasticity (E) of the swelling p(HEA/NMMA)-CuS hydrogel were detected before and after the photocatalytic degradation of SMX. Results (Table S1) reflected that the framework and elasticity modulus (E) of p(HEA/NMMA)-CuS hydrogel were almost unchanged in the scope of deviation allowed. Furthermore, no obvious degradation products of the composite hydrogel were observed as Fig. S13 shown, and the same results with the liquid phase detection under the condition of different wavelength as well as different mobile phase proportion. These probably demonstrated that p(HEA/NMMA)-CuS composite hydrogel possessed good stability and reutilization under visible light irradiation.

It should be noted that there are some shortcomings in this study, we temporarily can't answer these questions because of the length of the article, the progress of the test or the restriction of the test methods. But these issues are likely to be implemented in future studies. Despite its preliminary character, this study clearly indicate that the novel composite hydrogel did achieve a good effect of adsorption and degradation of organic matter, and overcome the difficulty of the post-recovery of the catalyst particles after water treatment and had good reutilization.

4. Conclusions

A novel hydrogel material was synthesized, with the function of adsorbing and photodegrading organic compounds, which named p(HEA/NMMA)-CuS hydrogel catalyst. Then, its performance was characterized and use for the adsorption and degradation of SMX in aqueous solution. The experimental results indicated that adsorption process fit well to Langmuir monolayer adsorption and followed a pseudo-second-order rate equation. Besides, the p(HEA/NMMA)-CuS hydrogel catalyst exhibited highly photocatalytic activity towards the degradation of SMX under visible light irradiation. The decomposition of SMX on p(HEA/NMMA)-CuS hydrogel in aqueous solution followed pseudo-first-order kinetics. Thereafter, decomposition process of SMX was proved by the identification of reactive radicals and photocatalytic products, hydroxyl radicals and eight primary intermediates of SMX degradation were detected. Their possible degradation pathways were presented and firmly established by theoretical calculations of frontier electron densities. Furthermore, p(HEA/NMMA)-CuS hydrogel catalyst was

promising for practical application owing to its good stability and regeneration. This work may promote the development and application of the novel hydrogel materials with catalysts.

Acknowledgments

This research was financially supported by research projects of the Major State Water Pollution Control and Treatment Technique Programs of China (No. 2017ZX07204-004 and 2013ZX07101-014).

Appendix A. Supplementary data

Supplementary data associated with this article can be found, in the online version, at http://dx.doi.org/10.1016/j.apcatb.2017.06.029.

6 Reference

[1] X. Yang, R.C. Flowers, H.S. Weinberg, P.C. Singer, Occurrence and removal of pharmaceuticals and personal care products (PPCPs) in an advanced wastewater reclamation plant, Water Res. 45 (2011) 5218–5228.
[2] L. Ji, F. Liu, Z. Xu, S. Zheng, D. Zhu, Adsorption of pharmaceutical antibiotics on template-synthesized ordered micro- and mesoporous carbons, Environ. Sci. Technol. 44 (2010) 3116–3122.
[3] M. Diugosz, P. Zmudzki, A. Kwiecien, K. Szczubialka, J. Krzek, M. Nowakowska, Photocatalytic degradation of sulfamethoxazole in aqueous solution using a floating TiO2-expanded perlite photocatalyst, J. Hazard. Mater. 298 (2015) 146–153.
[4] Y.K. Lan, T.C. Chen, H.J. Tsai, H.C. Wu, J.H. Lin, I.K. Lin, J.F. Lee, C.S. Chen, Adsorption behavior and mechanism of antibiotic sulfamethoxazole on carboxylic-functionalized carbon nanofibers-encapsulated Ni magnetic nanoparticles, Langmuir 32 (2016) 9530–9539.
[5] P. Shi, N. Ye, Investigation of the adsorption mechanism and preconcentration of sulfonamides using a porphyrin-functionalized Fe3O4-graphene oxide nanocomposite, Talanta 143 (2015) 219–225.
[6] A. Ghauch, G. Ayoub, S. Naim, Degradation of sulfamethoxazole by persulfate assisted micrometric Fe0 in aqueous solution, Chem. Eng. J. 228 (2013) 1168–1181.
[7] P.J.M. Reis, A.C. Reis, B. Ricken, B.A. Kolvenbach, C.M. Manaia, P.F.X. Corvini, O.C. Nunes, Biodegradation of sulfamethoxazole and other sulfonamides by Achromobacter denitrificans PR1, J. Hazard. Mater. 280 (2014) 741–749.
[8] B. Sun, F. Lian, Q. Bao, Z. Liu, Z. Song, L. Zhu, Impact of low molecular weight organic acids (LMWOAs) on biochar micropores and sorption properties for sulfamethoxazole, Environ. Pollut. 214 (2016) 142–148.
[9] I. Braschi, A. Martucci, S. Blasioli, L.L. Mzini, C. Ciavatta, M. Cossi, Effect of humic monomers on the adsorption of sulfamethoxazole sulfonamide antibiotic into a high silica zeolite Y: an interdisciplinary study, Chemosphere 155 (2016) 444–452.
[10] O. Ozay, S. Ekici, Y. Baran, N. Aktas, N. Sahiner, Removal of toxic metal ions with magnetic hydrogels, Water Res. 43 (2009) 4403–4411.
[11] M. Khan, I.M.C. Lo, A holistic review of hydrogel applications in the adsorptive removal of aqueous pollutants: recent progress, challenges, and perspectives, Water Res. 106 (2016) 259–271.
[12] C. Li, G. Chen, J. Sun, J. Rao, Z. Han, Y. Hu, W. Xing, C. Zhang, Doping effect of phosphate in Bi2WO6 and universal improved photocatalytic activity for removing various pollutants in water, Appl. Catal. B: Environ. 188 (2016) 39–47.
[13] Y. Ying, J.C. Yu, J.G. Yu, Y.C. Kwok, Y.K. Che, J.C. Zhao, D. Lu, W.K. Ge, P.K. Wong, Enhancement of photocatalytic activity of mesoporous TiO2 by using carbon nanotubes, Appl. Catal. A: Gen. 289 (2005) 186–196.
[14] K. Vinodgopal, D.E. Wynkoop, P.V. Kamat, Environmental photochemistry on semiconductor surfaces: photosensitized degradation of a textile azo dye, acid orange 7, on TiO2 particles using visible light, Environ. Sci. Technol. 30 (1996) 1660–1666.
[15] B. Luo, D. Xu, D. Li, G. Wu, M. Wu, W. Shi, M. Chen, Fabrication of a Ag/Bi3TaO7 plasmonic photocatalyst with enhanced photocatalytic activity for degradation of tetracycline, ACS Appl. Mater. Interfaces 7 (2015) 17061–17069.
[16] M.I. Litter, Heterogeneous photocatalysis: transition metal ions in photocatalytic systems, Appl. Catal. B: Environ. 23 (1999) 89–114.
[17] H.Q. Jiang, H. Endo, H. Natori, M. Nagai, K. Kobayashi, Fabrication and photoactivities of spherical-shaped BiVO4 photocatalysts through solution combustion synthesis method, J. Eur. Ceram. Soc. 28 (2008) 2955–2962.
[18] T. Paul, M.L. Machesky, T.J. Strathmann, Surface complexation of the zwitterionic fluoroquinolone antibiotic ofloxacin to nano-anatase TiO2 photocatalyst surfaces, Environ. Sci. Technol. 48 (2014) 11736 (vol 46, pg 11896, 2012).
[19] A. Ren, C. Liu, Y. Hong, W. Shi, S. Lin, P. Li, Enhanced visible-light-driven photocatalytic activity for antibiotic degradation using magnetic NiFe2O4/Bi2O3 heterostructures, Chem. Eng. J. 258 (2014) 301–308.
[20] U.T.D. Thuy, N.Q. Liem, C.M.A. Parlett, G.M. Lalev, K. Wilson, Synthesis of CuS and CuS/ZnS core/shell nanocrystals for photocatalytic degradation of dyes under visible light, Catal. Commun. 44 (2014) 62–67.
[21] M. Zhang, W.J. Luo, Z. Wei, W.J. Jiang, D. Liu, Y.F. Zhu, Separation free C3N4/SiO2 hybrid hydrogels as high active photocatalysts for TOC removal, Appl. Catal. B: Environ. 194 (2016) 105–110.
[22] J. Kundu, D. Pradhan, Controlled synthesis and catalytic activity of copper sulfide nanostructured assemblies with different morphologies, ACS Appl. Mater. Interfaces 6 (2014) 1823–1834.
[23] Z. Sun, X. Liu, Q. Yue, H. Jia, P. Du, Cadmium sulfide nanorods decorated with copper sulfide via one-step cation exchange approach for enhanced photocatalytic hydrogen evolution under visible light, ChemCatChem 8 (2016) 157–162.
[24] X.S. Hu, Y. Shen, L.H. Xu, L.M. Wang, L.S. Lu, Y.T. Zhang, Preparation of flower-like CuS by solvothermal method for photocatalytic, UV protection and EMI shielding applications, Appl. Surf. Sci. 385 (2016) 162–170.
[25] M.N. Chong, B. Jin, C.W.K. Chow, C. Saint, Recent developments in photocatalytic water treatment technology: a review, Water Res. 44 (2010) 2997–3027.
[26] W. Jiang, W. Luo, R. Zong, W. Yao, Z. Li, Y. Zhu, Polyaniline/carbon nitride nanosheets composite hydrogel: a separation-free and high-efficient photocatalyst with 3D hierarchical structure, Small 12 (2016) 4370–4378.
[27] M.N. Chong, V. Vimonses, S. Lei, B. Jin, C. Chow, C. Saint, Synthesis and characterisation of novel titania impregnated kaolinite nano-photocatalyst, Microporous Mesoporous Mater. 117 (2009) 233–242.
[28] H.Y. Zhu, X.P. Gao, Y. Lan, D.Y. Song, Y.X. Xi, J.C. Zhao, Hydrogen titanate nanofibers covered with anatase nanocrystals: a delicate structure achieved by the wet chemistry reaction of the titanate nanofibers, J. Am. Chem. Soc. 126 (2004) 8380–8381.
[29] M. Zhang, W.J. Jiang, D. Liu, J. Wang, Y.F. Liu, Y.Y. Zhu, Y.F. Zhu, Photodegradation of phenol via C3N4-agar hybrid hydrogel 3D photocatalysts with free separation, Appl. Catal. B: Environ. 183 (2016) 263–268.
[30] Z.P. Dong, X.D. Le, X.L. Li, W. Zhang, C.X. Dong, J.T. Ma, Silver nanoparticles immobilized on fibrous nano-silica as highly efficient and recyclable heterogeneous catalyst for reduction of 4-nitrophenol and 2-nitroaniline, Appl. Catal. B: Environ. 158 (2014) 129–135.
[31] L. Bromberg, W.R. Creasy, D.J. McGarvey, E. Wilusz, T.A. Hatton, Nucleophilic polymers and gels in hydrolytic degradation of chemical warfare agents, ACS Appl. Mater. Interfaces 7 (2015) 22001–22011.
[32] G.Y. Zhou, J.M. Luo, C.B. Liu, L. Chu, J.H. Ma, Y.H. Tang, Z.B. Zeng, S.L. Luo, A highly efficient polyampholyte hydrogel sorbent based fixed-bed process for heavy metal removal in actual industrial effluent, Water Res. 89 (2016) 151–160.
[33] L. Zeng, X.Y. Guo, C. He, C.Y. Duan, Metal-organic frameworks versatile materials for heterogeneous photocatalysis, ACS Catal. 6 (2016) 7935–7947.
[34] T. Zhang, W. Lin, Metal-organic frameworks for artificial photosynthesis and photocatalysis, Chem. Soc. Rev. 43 (2014) 5982–5993.
[35] N. Sahiner, Soft and flexible hydrogel templates of different sizes and various functionalities for metal nanoparticle preparation and their use in catalysis, Prog. Polym. Sci. 38 (2013) 1329–1356.
[36] Y. Zhang, Z. Li, Heavy metals removal using hydrogel-supported nanosized hydrous ferric oxide: synthesis, characterization, and mechanism, Sci. Total Environ. 580 (2017) 776–786.
[37] S.-G. Wang, X.-F. Sun, X.-W. Liu, W.-X. Gong, B.-Y. Gao, N. Bao, Chitosan hydrogel beads for fulvic acid adsorption: behaviors and mechanisms, Chem. Eng. J. 142 (2008) 239–247.
[38] M. Wang, G. Fang, P. Liu, D. Zhou, C. Ma, D. Zhang, J. Zhan, Fe3O4@β-CD nanocomposite as heterogeneous Fenton-like catalyst for enhanced degradation of 4-chlorophenol (4-CP), Appl. Catal. B: Environ. 188 (2016) 113–122.
[39] Y. Guo, J. Li, Z. Gao, X. Zhu, Y. Liu, Z. Wei, W. Zhao, C. Sun, A simple and effective method for fabricating novel p-n heterojunction photocatalyst g-C3N4/Bi4Ti3O12 and its photocatalytic performances, Appl. Catal. B: Environ. 192 (2016) 57–71.
[40] H. Liu, P. Sun, M. Feng, H. Liu, S. Yang, L. Wang, Z. Wang, Nitrogen and sulfur co-doped CNT-COOH as an efficient metal-free catalyst for the degradation of UV filter BP-4 based on sulfate radicals, Appl. Catal. B: Environ. 187 (2016) 1–10.
[41] Y. Li, X. Qiao, Y.-n. Zhang, C. Zhou, H. Xie, J. Chen, Effects of halide ions on photodegradation of sulfonamide antibiotics: formation of halogenated intermediates, Water Res. 102 (2016) 405–412.
[42] S. Gorai, D. Ganguli, S. Chaudhuri, Morphological control in solvothermal synthesis of copper sulphides on copper foil, Mater. Res. Bull. 42 (2007) 345–353.
[43] M. Basu, A.K. Sinha, M. Pradhan, S. Sarkar, Y. Negishi, Govind, T. Pal, Evolution of hierarchical hexagonal stacked plates of CuS from liquid–liquid interface and its photocatalytic application for oxidative degradation of different dyes under indoor lighting, Environ. Sci. Technol. 44 (2010) 6313–6318.
[44] Y. Shi, Y. Hu, L. Zhang, Z. Yang, Q. Zhang, H. Cui, X. Zhu, J. Wang, J. Chen, K. Wang, Palygorskite supported BiVO4 photocatalyst for tetracycline hydrochloride removal, Appl. Clay Sci. 137 (2017) 249–258.
[45] P. Qiu, J. Yao, H. Chen, F. Jiang, X. Xie, Enhanced visible-light photocatalytic decomposition of 2,4-dichlorophenoxyacetic acid over ZnIn2S4/g-C3N4 photocatalyst, J. Hazard. Mater. 317 (2016) 158–168.

[46] S.K. De, N.R. Aluru, B. Johnson, W.C. Crone, D.J. Beebe, J. Moore, Equilibrium swelling and kinetics of pH-responsive hydrogels: models, experiments, and simulations, J. Microelectromech. Syst. 11 (2002) 544–555.
[47] T. Traitel, J. Kost, S.A. Lapidot, Modeling ionic hydrogels swelling: characterization of the non-steady state, Biotechnol. Bioeng. 84 (2003) 20–28.
[48] E.S. Dragan, Design and applications of interpenetrating polymer network hydrogels. A review, Chem. Eng. J. 243 (2014) 572–590.
[49] H. Gong, W. Chu, Determination and toxicity evaluation of the generated products in sulfamethoxazole degradation by UV/CoFe2O4/TiO2, J. Hazard. Mater. 314 (2016) 197–203.
[50] B. Li, T. Zhang, Biodegradation and adsorption of antibiotics in the activated sludge process, Environ. Sci. Technol. 44 (2010) 3468–3473.
[51] A. Fujishima, T.N. Rao, D.A. Tryk, Titanium dioxide photocatalysis, J. Photochem. Photobiol. C: Photochem. Rev. 1 (2000) 1–21.
[52] P. Rodriguez-Escales, X. Sanchez-Vila, Fate of sulfamethoxazole in groundwater: conceptualizing and modeling metabolite formation under different redox conditions, Water Res. 105 (2016) 540–550.
[53] G. Liu, X. Li, B. Han, L. Chen, L. Zhu, L.C. Campos, Efficient degradation of sulfamethoxazole by the Fe(II)/HSO5(−) process enhanced by hydroxylamine: efficiency and mechanism, J. Hazard. Mater. 322 (2016) 461–468.
[54] M. Wang, D.E. Helbling, A non-target approach to identify disinfection byproducts of structurally similar sulfonamide antibiotics, Water Res. 102 (2016) 241–251.
[55] A.G. Trovó, R.F.P. Nogueira, A. Agüera, A.R. Fernandez-Alba, C. Sirtori, S. Malato, Degradation of sulfamethoxazole in water by solar photo-Fenton. Chemical and toxicological evaluation, Water Res. 43 (2009) 3922–3931.